Nanoscale

Surface Engineering of Pt Nanocatalysts with Transition Metal Oleates for Selective Catalysis: A Case Study on the Hydrogenation of α,β-Unsaturated Aldehydes

Journal:	*Nanoscale*
Manuscript ID	NR-ART-10-2024-004084.R1
Article Type:	Paper
Date Submitted by the Author:	28-Nov-2024
Complete List of Authors:	Kwon, Soon Gu; Argonne National Laboratory Chattopadhyay, Soma; Elgin Community College Shibata, Tomohiro; Argonne National Laboratory Krylova, Galyna; Argonne National Laboratory Sahoo, Sanjubala; University of Connecticut, Department of Materials Science and Engineering Filatov, Alexander; The University of Chicago, Department of Chemistry Adhikari, Shiba; Argonne National Laboratory Hood, Zachary; Argonne National Laboratory, Omotosho, Khalil; University of North Texas Berman, Diana; University of North Texas, Materials Science and Engineering Bunel, Emilio; Pontificia Universidad Catolica de Chile, Departamento de Química Inorgánica Jellinek, Julius; Argonne National Laboratory, Chemical Sciences and Engineering Division Shevchenko, Elena; Argonne National Laboratory, Center for Nanoscale Materials

Surface Engineering of Pt Nanocatalysts with Transition Metal Oleates for Selective Catalysis: A Case Study on the Hydrogenation of α,β-Unsaturated Aldehydes

*Soon Gu Kwon,[†] Soma Chattopadhyay,[@,§] Tomohiro Shibata,[§] Galyna Krylova,[†] Sanjubala Sahoo,[‡,$] Alexander Filatov,[#] Shiba Adhikari,[‖] Zachary David Hood,[‖] Khalil Omotosho,[&] Diana Berman,[&] Emilio Bunel,[‡,^] Julius Jellinek,[‡] and Elena V. Shevchenko[†,#,≠,]**

[†]*Center for Nanoscale Materials,* [‡]*Chemical Sciences and Engineering Division, and* [§]*CSRRI-IIT, MRCAT, Argonne National Laboratory, Argonne, Illinois, 60439 USA*

[@]*Math, Science and Engineering Department, Elgin Community College, Elgin, Illinois, 60123 USA*

[#]*Department of Chemistry, University of Chicago, Chicago, Illinois 60637 USA*

[‖] *Applied Materials Division, Argonne National Laboratory, Argonne, Illinois 60439, USA*

[&]*Department of Materials Science and Engineering, The University of North Texas, Denton, Texas, 76203 USA*

[$]*Department of Materials Science & Engineering and Institute of Materials Science, University of Connecticut, Storrs, Connecticut, 06269 USA*

[^]*School of Chemistry and Chemistry and Pharmacy, Catholic University of Chile, Santiago, 8331150 Chile*

[≠]*James Franck Institute, University of Chicago, Chicago, Illinois 60637 USA*

*Corresponding Author: eshevchenko@anl.gov

Abstract

Selective and active catalysts enable effective use of feedstocks, reduced energy consumption and waste generation. Tuning the electronic structure of heterogeneous metal nanocatalysts via their surface modifications is a promising strategy to design highly selective and active catalysts for the synthesis of harder to make and more cost-efficient products. We introduce transition metal oleates as a new class of ligands to engineer the catalytically active and very selective surface in organic solvents. Using citral hydrogenation and 5 nm Pt NPs as a model reaction and model catalytic system, respectively, we show that surface engineering of Pt nanocatalysts with metal oleates allows synthesis of desired partially hydrogenated product (geraniol) with ~90% conversion with selectivity over 93%. We demonstrate that the selective synthesis of the unsaturated alcohols catalyzed by Pt NPs modified by adsorption of the transition metal salts cannot be explained by widely accepted mechanism of preferred coordination of C=O groups by Lewis acids (e.g. partially oxidized transition surface metals). Our results indicate that C=O groups

prefer to bind to negatively charged surfaces. We propose the explanation on how the adsorption of transition metal oleates can results in the increased electron density at the surface of Pt nanoparticles. Our study not only provides reliable solutions to selective hydrogenation but opens a new possibility of using metal oleate for the electronic ligand effect.

Introduction

In modern industry, catalysts play a crucial role in 90% of chemical processes.[1] While their importance continues to grow, the focus of catalysis is shifting from merely enhancing activity to improving selectivity, aligning with the global shift from economic growth to sustainability.[2-6] The principles of green chemistry emphasize the need for catalysts that offer both high selectivity and good recyclability, integrating the benefits of both homogeneous and heterogeneous catalysts.[7-9]

Nanoparticles (NPs) have emerged as an attractive solution to meet this requirement.[10-18] Their high surface-to-volume ratio not only enhances economic efficiency but also facilitates extensive inorganic-organic interface interactions, providing versatile ways to modify their catalytic properties.[19, 20] The influence of organic ligands on catalytic NPs is generally discussed in terms of their steric and electronic effects. [15, 20-24] The steric effect arises from the crowding of molecules on the NP surface, where densely adsorbed ligands allow substrate molecules to bind exclusively to the active site, thereby improving selectivity. [25, 26] The electronic effect involves charge transfer between NPs and surface-adsorbed species. [24, 27, 28] This modified electronic structure can alter the energetics of catalytic reactions, favoring pathways that are otherwise thermodynamically unfavorable.

The selective hydrogenation of α,β-unsaturated aldehydes is a classic model reaction for studying chemoselectivity (Scheme 1).[26, 29-32] Among the three possible hydrogenation products, the target compound is the unsaturated alcohol, which holds high synthetic utility and market value. However, hydrogenating the C=C bond is significantly easier than the C=O bond.[26, 33] Therefore, achieving high selectivity requires developing methods to inhibit the hydrogenation of the C=C bond (pathways a and b) while allowing the hydrogenation of the C=O bond to proceed.

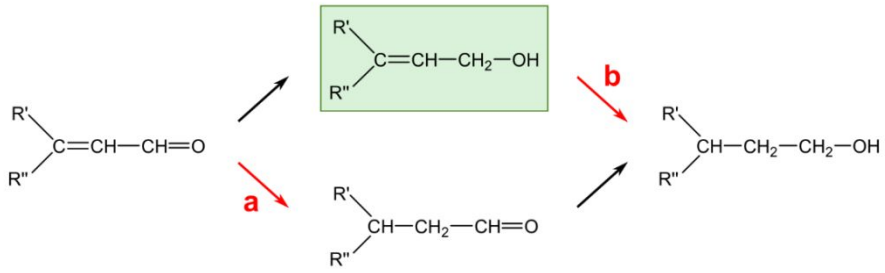

Scheme 1. Hydrogenation reaction pathways of α,β-unsaturated aldehyde.

Previous studies have explored both steric and electronic effects in blocking C=C bond hydrogenation. The steric effect, achieved through thiol or amine self-assembled monolayers (SAMs) on the catalyst surface, can prevent the C=C bond from accessing the active site.[26, 34] Electronic effect induced by adding ionic metal compounds as promoters was actively discussed until 1990s.[35-37] Metal cations absorbed on the catalyst surface were believed to serve as adsorption sites for the C=O bond via the oxygen atom, thereby promoting its hydrogenation. These studies were mainly conducted in polar solvent mixtures (e.g. ethanol/water). Similarly, electron transfer in bimetallic systems such as Pt-Fe, Pt-Ni, and Pt-Co was suggested to induce a partial positive charge on non-catalytic atoms, enhancing their ability to interact with the C=O bond and facilitate its hydrogenation.[38, 39] In dilute alloy catalysts, a third mechanism known as the ensemble effect was reported by Sachtler *et al*.[40] Larger ensembles of metal atoms can favor the binding of C=C bonds, which is accompanied by the binding of C=O bonds due to the structure of the citral molecule. Conversely, smaller ensembles of metal atoms on the surface of dilute alloys can favor the "vertical" binding of C=O bonds.[40-43]

The variety of approaches discussed above highlights the complex nature of interfacial effects on catalytic surface selectivity. From previous studies, we have identified several key issues. First, α,β-unsaturated aldehydes are prone to nucleophilic addition by amines and thiols, which limits the choice of ligands for inducing steric effects.[44] Second, controlling the surface composition of alloy NPs is challenging. For instance, oxidation and leaching of Co atoms from the surface of $CoPt_3$ NPs can occur even under mild conditions.[45, 46] Consequently, the selectivity of alloy nanoparticle catalysts may suffer from potential durability and inconsistency problems.

In this study, we demonstrate that the addition of metal oleate to Pt NPs enhances their selectivity while maintaining high activity in the hydrogenation of α,β-unsaturated aldehydes. We observed that selectivity of Pt NPs increased from zero to as high as 93%, and the yield could be optimized up to 83% in our model citral hydrogenation reaction. These results indicate that surface modification of Pt NPs with transition metal oleates (e.g. $Fe(oleate)_3$ and $Co(oleate)_2$) can lead to design of catalysts that significantly overperformed the performance of corresponding alloyed NPs (e.g. FePt or $CoPt_3$). Our results indicate that the increase in selectivity for C=O hydrogenation does not occur through the adsorption of the C=O bond of citral molecules by positively charged transition metal cations on the catalytic surface. Using X-ray photoelectron spectroscopy (XPS), Fourier-transform infrared spectroscopy (FTIR), and X-ray absorption spectroscopy, we confirmed that Pt NPs become negatively charged due to charge transfer from $Fe(oleate)_3$ adsorbed on their surface. Furthermore, density functional theory (DFT) calculations showed that C=O bond hydrogenation is energetically favored over C=C bond hydrogenation on negatively charged Pt NPs. Our study not only provides a reliable solution for selective hydrogenation but also opens new possibilities for using metal oleates to achieve electronic ligand effects in nonpolar solvents.

Results and Discussion

The hydrogenation of citral was conducted in a nonpolar solvent such as dodecane using alkylamine-capped 3.5 nm Pt NPs as the catalyst (Figure 1a, see Experimental Details). Cations of 3d transition metals (M^{n+}) were introduced to the reaction in the form of oleate compounds [$M(oleate)_n$]. The metal oleates are soluble in organic solvents that allows for testing the effect of the concentration in a broad concentration range. The results from hydrogenation reactions with different metal oleates as additives are presented in Figure 1b (for compositional data and reaction pathways, see Figure S1 and Scheme S1 in the Supporting Information). Without any additives, the Pt NPs catalyzed both C=C and C=O hydrogenation indiscriminately, resulting in 100% conversion and zero selectivity. However, the addition of metal oleates significantly altered their catalytic behavior, increasing selectivity to as high as 93% while lowering conversion. Among the metal oleates tested, $Fe(oleate)_3$ exhibited the highest yield. By optimizing the concentrations of both Pt and $Fe(oleate)_3$, the yield was further improved to 83%.

We observed a clear qualitative relationship between additive concentration and the catalytic properties of Pt NPs. Figure 1c illustrates the effect of additive concentration on conversion and selectivity. With a fixed Pt concentration of 3.1 mM, selectivity rapidly saturates as the concentration of $Fe(oleate)_3$ increases. An inverse relationship between conversion and selectivity is evident, where an increase in the latter accompanies a decrease in the former. Similar saturation behaviors are observed in reactions with $Co(oleate)_2$ (see Figure S2 in the Supplementary Information).

When plotted on a semi-log scale, the selectivity curve exhibits a sigmoidal shape, with the saturation region beginning in the range of 1–10 mM [Fe^{3+}] (inset in Figure 1c). This characteristic sigmoidal curve of selectivity fits well with the Hill–Langmuir equation (Figure S3 in the Supplementary Information), which describes an adsorption equilibrium between a protein (P) with n binding sites and a ligand (L): $P + nL \rightleftharpoons PL_n$.[47] Based on the fit result, we can hypothesize that by substituting Pt NPs for the protein *P* and $Fe(oleate)_3$ for the ligand (*L)*, the selectivity reflects the equilibrium ratio of $Fe(oleate)_3$-decorated Pt NPs (PL_n). This hypothesis is further supported by the data in Figure 1d. When the amount of Pt is increased tenfold while maintaining a constant molar ratio of Pt to $Fe(oleate)_3$, conversion increases monotonically from 23% to 96%. Conversely, selectivity shows only a small decrease of 7%. Turnover numbers (TON) that correspond to the data in Figure 1c and Figure 1d are estimated and shown in Figure S4 in Supporting Information. Under the standard reaction condition with [Pt] = 3.1 mM, TON is above 140 when [Fe] is less than 0.05 mM and drops down to 29 with [Fe] = 111 mM ([Fe]/[Pt] = 35.8). We investigated the possibility of reduction and alloying of metal cations with Pt NPs during the hydrogenation reaction. XPS data for Co and Fe species of Pt NPs modified with $Co(oleate)_2$ and $Fe(oleate)_3$ before and after hydrogenation reaction show negligible changes in terms of their oxidation states (Figure S5 in the Supplementary Information SI). Additionally, when FePt and $CoPt_3$ NPs were used as catalysts instead of

Pt NPs, despite having the same Pt concentration, they exhibited significantly different catalytic properties for citral hydrogenation, with yields of 9% and 0% of products with hydrogenated C=O bond for FePt and $CoPt_3$ NPs, respectively (Figure S6 in the Supplementary Information). These observations effectively exclude the possibility of an alloying effect in our system.

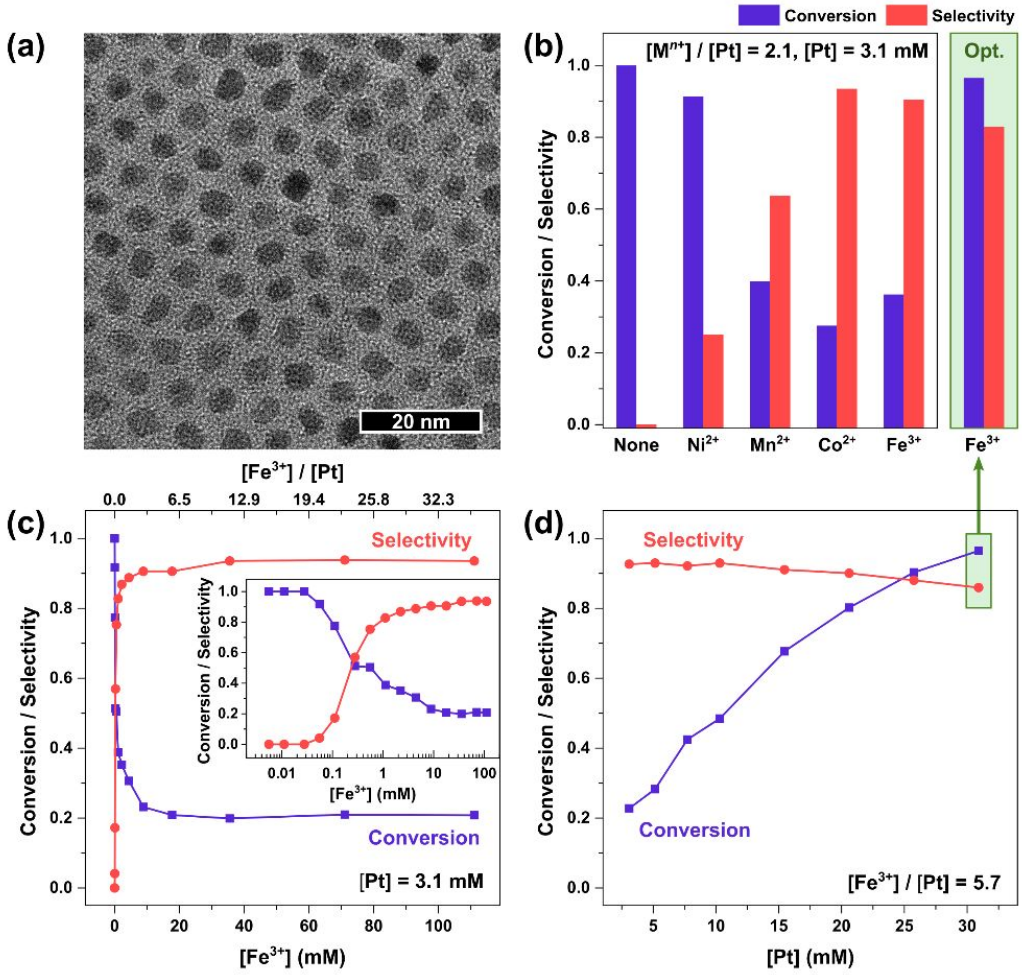

Figure 1. (a) Transmission electron microscopy image of Pt NPs used as catalyst for citral hydrogenation. (b) Conversion and selectivity for unsaturated alcohol from the reactions with different metal oleate additives. The concentrations of Pt and metal cations are fixed for all reactions in the left panel as indicated. In the right panel, the data from the optimal condition in panel d is shown. (c) Plots for conversion and selectivity as functions of $[Fe^{3+}]$ with Pt concentration fixed at 3.1 mM. In the inset, the same data are re-plotted in semi-log scale. (d) Plots for conversion and selectivity as functions of Pt concentration with the molar ratio of cation to Pt fixed at 5.7.

The comparative binding of citral and $Fe(oleate)_3$ onto the surface of Pt NPs was studied using FTIR to investigate the effect of metal oleate additive in greater detail (Figure 2a). Citral exhibits a strong peak at 1685.5 cm^{-1} attributed to the stretching vibration of the C=O bond.[48] As the concentration of Pt NPs increases to a [citral]:[Pt] ratio of 1:7.5, the C=O peak disappears, indicating the binding of the C=O group to the Pt surface, which suppresses the bond vibration.[35, 49] However, upon the addition of $Fe(oleate)_3$ to the

same mixture, the C=O peak reappears, suggesting the desorption of free citral. These observations imply that the presence of $Fe(oleate)_3$ reduces the binding affinity of citral to the Pt NP surface, altering the adsorption equilibrium.

To further explore this hypothesis, mixtures of citral and Pt NPs with varying amounts of $Fe(oleate)_3$ were compared (Figure 2b). After one day, Pt NPs precipitated except in mixtures with a high concentration of $Fe(oleate)_3$, due to ligand exchange between the long alkyl-chain surfactant and citral. Notably, Pt NPs capped with alkylthiol, which binds more strongly than alkylamine, maintained their colloidal stability without the additive.[19, 50] Consequently, we deduce that the binding affinity of citral to pristine Pt NPs is intermediate between that for amine and thiol and can be significantly lowered by the adsorption of metal oleate onto the NPs.

We investigated the interaction between Pt NPs and $Fe(oleate)_3$ using synchrotron X-ray absorption spectroscopy. X-ray absorption near edge structure (XANES) spectra of the Fe K-edge were measured for $Fe(oleate)_3$ mixed with varying amounts of Pt NPs (Figure 3a). As the molar ratio of Pt increases, the spectra reveal significant changes in the coordination environment of the Fe atoms, with more Fe complex molecules adsorbing onto the NP surface. This is accompanied by a decrease in Fe-O correlation, as observed in the extended X-ray absorption fine structure (EXAFS) data (Figure 3b). EXAFS fitting analysis confirms the formation of Fe-Pt bonds upon adsorption (Table S1 in the Supplementary Information).

It is known that carboxylate ligands coordinated to Fe^{3+} ions generally favor a bidentate structure, either in chelate or bridging modes. However, conversion between monodentate and bidentate structures is also possible depending on the chemical environment of the complex.[51, 52] We hypothesize that upon the adsorption of $Fe(oleate)_3$ onto the surface of Pt NPs, the coordination geometry of the oleate ligand changes from bidentate with two Fe-O bonds to monodentate with one Fe-O bond and/or bridging bidentate with both Fe-O and Pt-O bonds. This structural change facilitates the formation of Fe-Pt bonds (see Scheme S2 in the Supplementary Information). This also explains the simultaneous decrease and increase in the coordination numbers for Fe-O and Fe-Pt bonds, respectively. It is worth noting that we tested different transition metal salts such as chlorides and acetylacetonates (Figure S7). However, iron and cobalt oleates provided the highest selectivity. This observation points out to the importance of the dissociation event of the metal salt and coordination geometry of the adsorbed species.

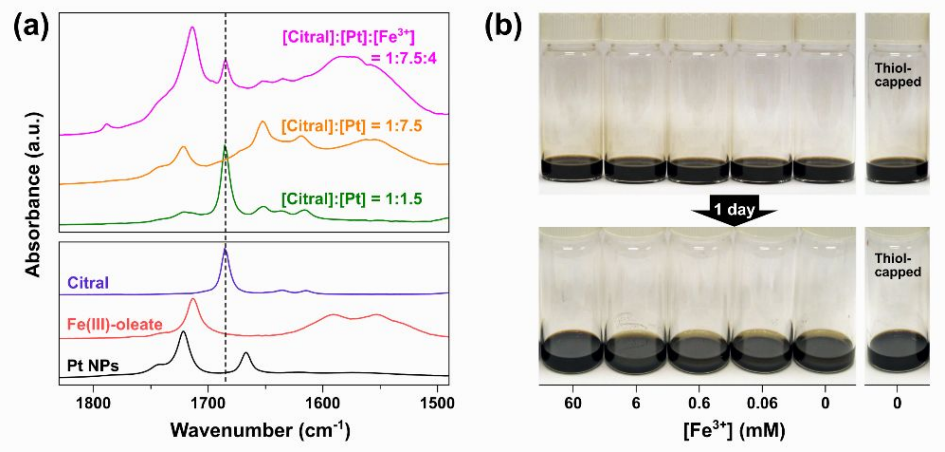

Figure 2. (a) FTIR spectra for citral, Pt NPs, and Fe(oleate)$_3$ solutions in *n*-dodecane (lower) and their mixtures with different molar ratios (upper). In all mixtures, [citral] = 25 mM. (b) Effect of varying concentration of Fe(oleate)$_3$ on precipitation of Pt NPs. In the rightmost vial, Pt NPs capped with *n*-dodecanethiol were used. In all mixtures, [citral] = 112 mM and [Pt] = 17.0 mM in *n*-dodecane.

The effect of Fe(oleate)$_3$ adsorption on the electronic structure of Pt NPs was measured using the XANES spectrum at the Pt L_3-edge (Figure 3c). The intensity of the white line at the L_3-edge reflects the d-band vacancy of Pt, serving as an indicator of charge transfer to the Pt NPs.[53, 54] With an excess amount of the additive in the solution, we observed a reduction in the white line intensity compared to pristine Pt NPs (Figure 3d). This corresponds to a 1.35% decrease in the normalized absorption scale, as estimated by Gaussian curve fitting (Table S2 in the Supplementary Information), confirming an increase in the electron density of Pt. Analysis of XPS data obtained for 3.5 nm Pt NPs and Pt NPs modified with metal oleates (Co(oleate)$_2$ and Fe(oleate)$_3$) indicate that Pt oxidation states undergo changes during surface modification (Figure S8). The signals corresponding to $4f_{5/2}$ and $4f_{7/2}$ peaks in unmodified 3.5 nm Pt NPs centered at 75.13 eV and 71.87 eV moved to 74.11 eV and 70.77 eV and 74.01 eV and 70.71 eV upon surface modification with Fe(oleate)$_3$ and Co(oleate)$_2$, respectively (Figure S8) that is indicative to more reduced state of Pt atoms at the surface of modified NPs. The combined evidence from X-ray absorption spectroscopy and XPS studies validates that the adsorption of Fe(oleate)$_3$ onto the surface of Pt NPs results in the NPs becoming negatively charged.

Before discussing how charge transfer from the Fe complex to Pt NPs modifies their catalytic properties, it is important to mention the classical mechanism for the effect of metal salt promoters on selective hydrogenation. As previously explained, metal cations adsorbed on the Pt surface selectively attract the lone electron pairs of oxygen on the C=O group, which facilitates the hydrogenation of its π bond.[35, 36] This model, however, is only feasible in aqueous and other polar solutions where the promoters are easily ionized. In an organic medium such as in our system, it is unlikely that the C=O group can form a dative bond with the metal cation, which is surrounded and ionically bound by bulky oleate anions, to promote

selectivity. In other words, the enhancement of selectivity in our system cannot be explained by the coordination of the C=O bond by positively charged species.

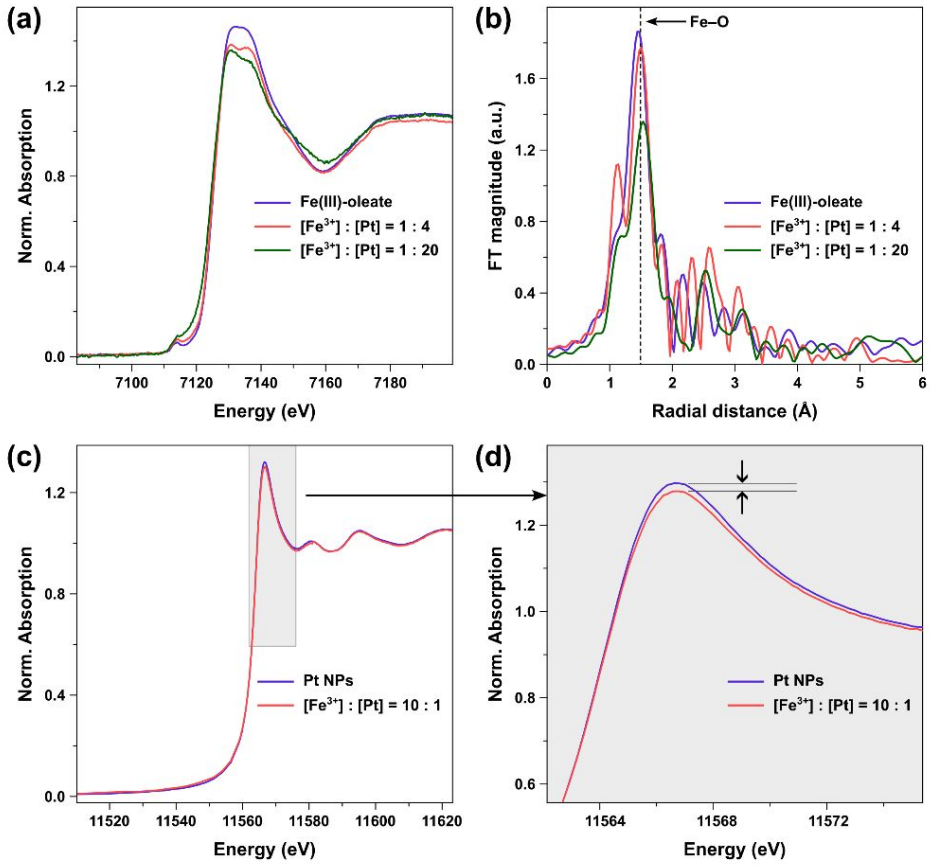

Figure 3. (a) Fe *K*-edge XANES spectra of $Fe(oleate)_3$ and its mixtures with Pt NPs. (b) k^2-weighted EXAFS data for the same samples as in panel a. (c) Pt L_3-edge XANES spectra of Pt NPs with and without $Fe(oleate)_3$. (d) Magnification of the area colored in grey in panel c.

We conducted density functional theory (DFT) calculations to characterize various adsorption configurations and their corresponding adsorption energies for a citral molecule on the surfaces of neutral and negatively charged 55-atom platinum clusters (Pt_{55}), which were selected as models for the Pt nanocatalyst (see the Experimental Details). Notably, the configurations depicted in Figure 4a, referred to as "horizontal" and "vertical," are directly relevant to the hydrogenation of the C=O bond and the C=C bond at the α,β-position.[35, 49] In the horizontal adsorption arrangement, both the C=O bond and the C=C bond can be activated. In contrast, in the vertical arrangement, only the C=O bond can be hydrogenated, resulting in selectivity. To emulate negatively charged Pt NPs, we placed four Fe atoms on the surface of the Pt_{55} cluster. The charge transfer from the Fe atoms to the Pt cluster occurs because the electronegativity of Pt (2.28 on the Pauling scale) is significantly higher than that of Fe (1.83). The Fe atoms were arranged at positions opposite the citral adsorption sites to minimize interactions between the Fe atoms and the citral

ligand. Our calculations confirmed that the net charge of the Pt_{55} network in the $Pt_{55}Fe_4$ complex is negative. The calculated citral adsorption energies for the different adsorption configurations are shown in Figure 4b. The adsorption of citral in the horizontal arrangement on the bare Pt_{55} has the highest adsorption energy at 2.607 eV. This value decreases significantly to 0.928 eV when citral is adsorbed horizontally on $Pt_{55}Fe_4$ (negatively charged Pt_{55}). In contrast, the adsorption energy in the vertical arrangement gets only slightly reduced from 0.994 eV on the bare Pt_{55} to 0.946 eV on $Pt_{55}Fe_4$, with the latter being higher than the corresponding value for horizontal adsorption on $Pt_{55}Fe_4$. These results indicate that supplying a negative charge to the cluster shifts the energetic preference from horizontal to vertical adsorption of citral. This finding aligns with earlier theoretical studies, which showed that charging Pt catalysts decreases C=C bond adsorption more than C=O bond adsorption due to the larger repulsive interaction experienced by the C=C bond.[39] Theoretical proposals suggest that enriching the surface with electrons can be achieved by interfacing platinum with electron-donating supports such as titania or carbon.[55] This enrichment can also be facilitated by using Pt (111) faces, employing metals with more extended d orbitals like osmium or iridium, or by avoiding open faces and steps in Pt catalysts.[55]

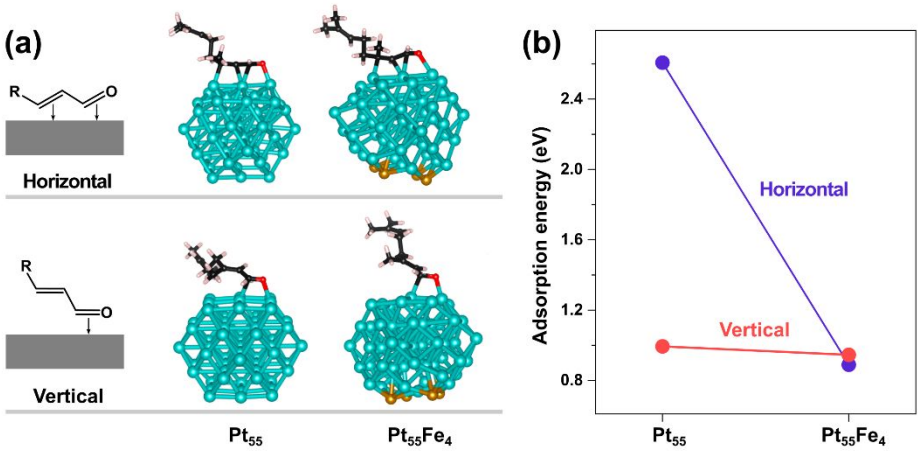

Figure 4. (a) DFT-calculated geometrically optimized structures of citral molecule adsorbed horizontally and vertically on Pt_{55} and $Pt_{55}Fe_4$ clusters. The color coding is as follows: Pt - cyan, Fe – brown, O – red, C - black, and H – tan. (b) Adsorption energies corresponding to the 4 adsorption configurations shown in panel (a).

Our calculated results align with our measured data and provide an explanation for them. The observed enhancement in selectivity for C=O hydrogenation, induced by the addition of $Fe(oleate)_3$ to the Pt NPs, and the increase in selectivity with the concentration of $Fe(oleate)_3$ (Figure 4) are consequences of the electron-donating effect of $Fe(oleate)_3$. The accompanying reduction in the reaction rate and conversion is due to the charge-transfer induced decrease in the binding energy of the substrate moleculemolecule. Weaker binding energy of the substrate molecules indicates that reactants do not readily interact with the catalyst that results in lower activity of the catalysts and hence lower activity of the catalysts. Indeed, we

experimentally observe that the increase of selectivity is accompanied by decrease in conversion of citral (Figure 1c). In order to achieve high conversion, it is required to increase the concentration of the catalysts, as we experimentally observed (Figure 1d). The calculated adsorption energy of citral on bare Pt_{55} in its preferred configuration is 2.607 eV, which falls between the adsorption energies of alkylthiol (above 3 eV)[50] and alkylamine (~1 eV).[24] On the negatively charged Pt_{55}, this value drops below 1 eV, which is less than that of alkylamine. These comparative adsorption energies are consistent with the experimentally observed binding affinities of citral, amine, and thiol (Figure 2).

To complement the DFT results, we conducted several control experiments to clarify the role of additives and the size effect of catalyst particles. First, we investigated whether surfactants other than metal oleate, with similar electron-donating effects, could enhance selectivity. Phosphine ligands are well-known soft Lewis bases with a strong binding affinity to the Pt surface.[56, 57] As shown in Figure 5a, when the concentration of trioctylphosphine (TOP) is plotted as the additive, the conversion and selectivity exhibit similar behaviors to those in Figure 1c, although the overall yield is much lower (Figure S8).

Unlike TOP, both trioctylphosphine oxide (TOPO) and oleic acid (OLEA), which are weak binding molecules for Pt NPs, show little to no effect on the catalytic reaction, consistent with previous studies (Figure 5b, left panel, Figure S8).[24] Additionally, we tested Pt black, with the particle size of 20 μm or smaller, instead of NPs as the catalyst (Figure 5b, right panel). Interestingly, reactions with and without $Fe(oleate)_3$ showed no difference, achieving 100% conversion and 0% selectivity. This suggests that the charging effect of metal oleate diminishes at the bulk scale and that $Fe(oleate)_3$ itself does not catalyze citral hydrogenation. This observation aligns with previous studies on intraparticle charge delocalization occurring between molecules bound to the surface of metallic NPs.[58] Overall, these control experiments corroborate that the effect of metal oleate is due to its electron-donating nature at the surface of Pt NPs.

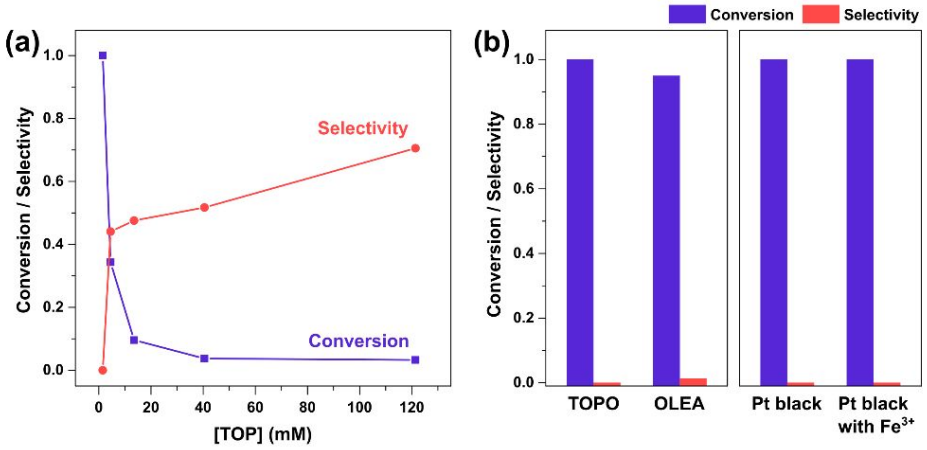

Figure 5. (a) Plots for conversion and selectivity as functions of [TOP] for citral hydrogenation using Pt NPs as catalyst and TOP as the additive. Pt concentration is fixed at 3.1 mM. (b) Conversion and selectivity for the reactions using Pt NPs with [Pt] = 3.1

mM (left panel) and Pt black with [Pt] = 100 mM (right panel) as catalyst. The concentrations of the additives are as follow; [TOPO] = 40.5 mM, [OLEA] = 31.7 mM, and [Fe(oleate)$_3$] = 6.4 mM.

Conclusions

We unveiled the interfacial electronic effect induced by metal salts in nonpolar organic solvents and demonstrated their applicability for the selective hydrogenation of α,β-unsaturated aldehyde to unsaturated alcohol using Pt NPs as the catalyst and metal oleate as the additive. Our findings reveal that metal oleate, unlike conventional Lewis basic ligands, can facilitate charge transfer to Pt NPs. This charge interaction between metal oleate and Pt NPs is strong enough to enhance catalytic properties, increasing selectivity from zero to as high as 93%. We also established a relationship between the increased electron density in Pt NPs and enhanced selectivity. Experimentally, we observed that the selectivity depends on Fe(oleate)$_3$ at the surface of Pt NPs, following the Hill–Langmuir equation, which describes the cooperativity of ligand binding to proteins. Experimental data are indicative to the charge transfer from adsorbed species originating from the addition of transition metal oleates to Pt NPs resulting in a negative charge at the Pt surface, which promotes the preferred adsorption of C=O groups and their selective hydrogenation. These experimental data are consistent with the data of DFT calculations on Pt_{55} clusters modified with Fe atoms. This mechanism differs from previously reported ideas, which suggested that a local positive surface charge was necessary for enhanced adsorption of C=O groups in α,β-unsaturated aldehydes. Broadly, this strategy for designing highly selective and active catalysts can be extended to other catalytic processes. Unlike common ligands such as alkylamine and alkylthiol, organic salts are relatively stable and inactive towards the substrate molecules. This stability makes the reaction system more reliable, especially in the presence of unwanted side reactions between the substrate and Lewis basic ligands. Consequently, metal oleate can serve as an excellent alternative or even superior substitute for conventional ligands in selective hydrogenation systems. We anticipate that the potential of using organic salts can be realized in other reaction systems in nonpolar organic solvents[59] that is important due to the solubility of substrate molecules, better stability of the catalysts, enhanced reaction rates, and synthetic versatility nonpolar solvents offer.

Experimental Section

Catalytic hydrogenation of citral. Pt, FePt, and $CoPt_3$ NPs as catalyst and metal oleate as the additive were synthesized following previously reported methods. [24, 60] Commercial Pt black (≤20 μm, 25 m^2 g^{-1}) was purchased from Aldrich. The NPs were thoroughly washed by repeated dispersion and precipitation to remove any residual surfactants that can interact with the substrate (see Figure S10 in SI). The hydrogenation reaction was carried out under H_2 atmosphere (200 psig) at room temperature for 3 hr in a stainless-steel reactor. During the reaction, the solution was stirred at 7000 rpm. In a standard condition, the reaction solution was prepared by dispersing Pt NPs in 1.0 mL dodecane containing 3.75 wt % (185

mM) of citral. The atomic concentration of Pt in the solution was measured by inductively coupled plasma (ICP) analysis.

Characterization. Transmission electron microscopy (TEM) measurement was performed by using a JEOL 2100F microscope operated at 200 kV. Composition of the solutions before and after hydrogenation reactions were analyzed by GC-MS system consisting of an Agilent 6890 GC system and a 5973 Network Selective Detector. FTIR spectrum was obtained by using a Bruker Vertex 70 spectrometer equipped with mercury cadmium telluride detector. Specimen for FTIR characterization was prepared by placing a drop of the sample solution on KBr pellet.

XPS measurement was performed by using a Shimadzu Kratos Axis Nova spectrometer with monochromatic Al Kα source (1486.6 eV). High-resolution spectra were collected using an analysis area of 0.3×0.7 mm^2 and 20 eV pass energy with the step size of 100 meV. Charge neutralization was performed using a co-axial, low energy (≈ 0.1 eV) electron flood source to avoid shifts in the recovered binding energy. C 1s peak of adventitious carbon was set at 284.8 eV to compensate for any remaining charge-induced shifts. The XPS spectra on unmodified Pt NPs were collected on a Thermo K-alpha XPS system with a spot size of 400 μm and a resolution of 0.1 eV. All spectra were processed using THermo Avantage, a software package provided by ThermoScientific. Specimen for XPS was prepared by drop-casting NPs in toluene on a zero-background offcut Si substrate.

X-ray absorption spectroscopy measurements on Fe *K*-edge and Pt L_3-edge were carried out at the MRCAT 10-ID beamline at the Advanced Photon Source, Argonne National Laboratory. The spectra were recorded in the transmission mode with samples deposited on Kapton tape. The spot size of the incident X-ray beam on the sample was 400×400 μm^2. Pt and Fe foils were measured as reference for every scan. Ten scans were recorded for each sample to ensure repeatability and averaged to improve statistics. XANES and EXAFS data were processed and analyzed by using ATHENA software.[61] We measured and averaged in analysis at least 10-12 scans for each edge and we fitted Pt and Fe EXAFS data simultaneously.

Computational details. The calculations were performed within the gradient-corrected DFT framework using the VASP package[62] with the PBE exchange-correlation functional[63] and plane-wave basis set kinetic energy cut-off value of 400 eV. The projector augmented-wave (PAW) method[64, 65] was used to account for the interactions of the valence electrons with the cores. The valence configurations of the atoms were Pt[$6s^1 5d^9$], Fe[$3d^7 4s^1$], O[$2s^2 2p^4$] and C[$2s^2 2p^2$]. The Brillouin zone integration was done at the gamma point. The energy convergence criterion used was 10^{-6} eV. The cuboctahedral form of the 55-atom Pt cluster, which is a fragment of the *fcc* bulk Pt, was chosen to model the Pt nanocatalyst. The adsorption of the geranial conformation of citral was considered. A large supercell of 25x25x25 $Å^3$ was utilized to minimize the interaction of the system with its periodic images. The bare Pt_{55} cluster, the free citral molecule, the cluster with the citral on it, the cluster with 4 Fe atoms on it, and the cluster with the citral

and 4 Fe atoms on it were fully optimized without symmetry constraints using gradient-based techniques as implemented in VASP. The resulting geometries were considered as converged when the residual forces were less than 0.02 eV/Å. The adsorption energies E_{ads} of the citral on the cluster without and with the Fe atoms on it were calculated as

$$E_{ads} = E_{Pt_{55}[Pt_{55}Fe_4]} + E_{citral} - E_{Pt_{55}-citral[Pt_{55}Fe_4-citral]},$$

where $E_{Pt_{55}[Pt_{55}Fe_4]}$ is the energy of the optimized Pt_{55} without or with the 4 Fe atoms on it, E_{citral} is the energy of the optimized free citral molecule, and $E_{Pt_{55}-citral[Pt_{55}Fe_4-citral]}$ is the energy of the optimized Pt_{55}-citral or $Pt_{55}Fe_4$-citral complex. The charge analysis was performed using the Bader scheme.[66]

ASSOCIATED CONTENT

Supporting Information. Compositional data for citral hydrogenation reactions; results on conversion and selectivity in citral hydrogenation reactions on Pt NPs modified with $Co(oleate)_2$; selectivity plot its fit result using the Hill–Langmuir equation as fitting function; X-ray photoelectron spectroscopy spectra of the solution using the corresponding metal oleate additives before and after hydrogenation reaction; compositional data for citral hydrogenations using 4 nm FePt and 4.5 nm $CoPt_3$ NPs as catalysts; EXAFS fitting result for Fe *K*-edge; coordination geometries of carboxylate ligand for free- and Pt-adsorbed $Fe(oleate)_3$; curve fitting result for the white line of Pt L_3-edge XANES spectra; compositional data for citral hydrogenation reactions corresponding for 3.5 nm Pt NPs modified with strongly and weakly bound organic ligands and results of catalytic tests on Pt black.

AUTHOR INFORMATION

Corresponding Author

* eshevchenko@anl.gov

Author Contributions

Elena V. Shevchenko and Soon Gu Kwon conceptualized the idea and planed the experimental work; Soon Gu Kwon and Galyna Krylova synthetized nanoparticles and conducted catalytic tests; Soon Gu Kwon, Soma Chattopadhyay and Tomohiro Shibata conducted synchrotron measurements and analyzed the data; Sanjubala Sahoo and Julius Jellinek conducted DFT calculations and theoretical analyses; Alexander Filatov, Shiba Adhikari and Zachary David Hood conducted XPS studies; Khalil Omotosho and Diana Berman conducted studies on surface modification of nanoparticles; Emilio Bunel directed catalytic studies; Elena V. Shevchenko, Soon Gu Kwon, Emilio Bunel and Julius Jellinek analyzed the results and prepared the manuscript.

Funding Sources

U.S. Department of Energy Office of Science User Facility, was supported by the U.S. DOE, Office of Basic Energy Sciences, under Contract No. DE-AC02-06CH11357. U.S. Department of Energy Office of Basic Energy Sciences, Division of Chemical Sciences, Geosciences and Biosciences, U.S. DOE under Contract No. DE-AC02-06CH11357. National Energy Research Scientific Computing Center (NERSC) supported by the Office of Science of the U.S. DOE under Contract No. DE-AC02-05CH11231.

ACKNOWLEDGMENT

The work performed at the Center for Nanoscale Materials, a U.S. Department of Energy (DOE) Office of Science User Facility, was supported by the U.S. DOE, Office of Basic Energy Sciences, under Contract No. DE-AC02-06CH11357. The work performed at Chemical Science and Engineering, Argonne National Laboratory was supported by the Office of Basic Energy Sciences, Division of Chemical Sciences, Geosciences and Biosciences, U.S. DOE under Contract No. DE-AC02-06CH11357. This research used the resources of the National Energy Research Scientific Computing Center (NERSC) supported by the Office of Science of the U.S. DOE under Contract No. DE-AC02-05CH11231. We also gratefully acknowledge use of the facilities of the Laboratory Computing Resource Center (LCRC) at Argonne National Laboratory.

REFERENCES

1. https://www.energy.gov/eere/amo/articles/technology-vision-2020-us-chemical-industry, 2020.
2. R. Noyori, *Nature Chemistry*, 2009, **1**, 5 - 6.
3. R. M. R. G. A. Somorjai, *Catalysis Today*, 2005, **100**, 201-215.
4. A. Schmid, J. S. Dordick, B. Hauer, A. Kiener, M. Wubbolts and B. Witholt, *Nature*, 2001, **409**, 258-268
5. T. H. a. J. K. N. Rod, *Surf. Sci.*, 2002, **500**, 678-698.
6. D.-H. Wang, K. M. Engle, B.-F. Shi and J.-Q. Yu, *Science*, 2010, **327**, 315-319.
7. I. Fechete, Y. Wang and J. C. Védrine, *Catalysis Today*, 2012, **189**, 2-27.
8. L. J. Durndell, C. M. A. Parlett, N. S. Hondow, M. A. Isaacs, K. Wilson and A. F. Lee, *Scientific Reports*, 2015, **5**, 9425.
9. M. Duval, G. Sagorin, A. Denicourt-Nowicki and A. Roucoux, *ACS Sustainable Chemistry & Engineering*, 2022, **10**, 5500-5506.
10. C. Pei, S. Chen, D. Fu, Z.-J. Zhao and J. Gong, *Chemical Reviews*, 2024, **124**, 2955-3012.
11. E. Gross and G. A. Somorjai, *Topics in Catalysis*, 2014, **57**, 812-821.
12. N. Z. Binghui Wu, *Nano Today*, 2013, **8**, 168-197.
13. W. Wu and E. V. Shevchenko, *Journal of Nanoparticle Research*, 2018, **20**, 255.
14. Y. Zhao, G. Fu and N. Zheng, *Catalysis Today*, 2017, **279**, 36-44.
15. C. Hu, R. Chen and N. Zheng, *Advanced Materials*, 2021, **33**, 2006159.
16. D. Astruc, F. Lu and J. R. Aranzaes, *Angewandte Chemie International Edition*, 2005, **44**, 7852-7872.
17. F. Zaera, *Chemical Reviews*, 2022, **122**, 8594-8757.
18. I. Schrader, S. Neumann, A. Šulce, F. Schmidt, V. Azov and S. Kunz, *ACS Catalysis*, 2017, **7**, 3979-3987.

19. K. Liu, R. Qin and N. Zheng, *Journal of the American Chemical Society*, 2021, **143**, 4483-4499.
20. L. Lu, S. Zou and B. Fang, *ACS Catalysis*, 2021, **11**, 6020-6058.
21. W. Zhang, R. Qin, G. Fu and N. Zheng, *Journal of the American Chemical Society*, 2023, **145**, 10178-10186.
22. J. W. Medlin, *Acc. Chem. Res.*, 2013, **47**, 1438-1445.
23. D. K. S. Carolyn A. Schoenbaum, J. Will Medlin, *Journal of Catalysis* 2013, **303**, 92-99.
24. S. G. Kwon, G. Krylova, A. Sumer, M. M. Schwartz, E. E. Bunel, C. L. Marshall, S. Chattopadhyay, B. Lee, J. Jellinek and E. V. Shevchenko, *Nano Letters*, 2012, **12**, 5382-5388.
25. S. T. Marshall, M. O'Brien, B. Oetter, A. Corpuz, R. M. Richards, D. K. Schwartz and J. W. Medlin, *Nature Materials*, 2010, **9**, 853.
26. K. R. Kahsar, D. K. Schwartz and J. W. Medlin, *Journal of the American Chemical Society*, 2014, **136**, 520-526.
27. G. Chen, C. Xu, X. Huang, J. Ye, L. Gu, G. Li, Z. Tang, B. Wu, H. Yang, Z. Zhao, Z. Zhou, G. Fu and N. Zheng, *Nature Materials*, 2016, **15**, 564.
28. D. W. a. A. Navrotsky, *PNAS*, 2015, **112**, 5314–5318
29. M. S. Ide, B. Hao, M. Neurock and R. J. Davis, *ACS Catalysis*, 2012, **2**, 671-683.
30. A. Giroir-Fendler, D. Richard and P. Gallezot, *Catalysis Letters*, 1990, **5**, 175-181.
31. S. Schauermann, *The Journal of Physical Chemistry Letters*, 2018, **9**, 5555-5566.
32. X. Lan and T. Wang, *ACS Catalysis*, 2020, **10**, 2764-2790.
33. Z. Ferhat, A. Derouault, J. Barrault and M. Bettahar, *Reaction Kinetics and Catalysis Letters*, 2002, **76**, 249-258.
34. B. Wu, H. Huang, J. Yang, N. Zheng and G. Fu, *Angewandte Chemie International Edition*, 2012, **51**, 3440-3443.
35. V. Ponec, *Applied Catalysis A: General*, 1997, **149**, 27-48.
36. D. Richard, J. Ockelford, A. Giroir-Fendler and P. Gallezot, *Catalysis Letters*, 1989, **3**, 53-58.
37. S. Galvagno, A. Donato, G. Neri, R. Pietropaolo and D. Pietropaolo, *Journal of Molecular Catalysis*, 1989, **49**, 223-232.
38. X. Li, S. Zhang, L. Zhu, J. Liu, H. Zhang, N. Zhao and B. H. Chen, *Materials Chemistry and Physics*, 2023, **294**, 127003.
39. L. Ning, M. Zhang, S. Liao, Y. Zhang, D. Jia, Y. Yan, W. Gu and X. Liu, *ChemCatChem*, 2021, **13**, 704-711.
40. W. M. H. Sachtler and R. A. V. Santen, in *Advances in Catalysis*, eds. D. D. Eley, H. Pines and P. B. Weisz, Academic Press, 1977, vol. 26, pp. 69-119.
41. P. Aich, H. Wei, B. Basan, A. J. Kropf, N. M. Schweitzer, C. L. Marshall, J. T. Miller and R. Meyer, *The Journal of Physical Chemistry C*, 2015, **119**, 18140-18148.
42. M. R. Ball, L. Proaño, I. Nezam, D.-C. Lee, F. Alamgir and C. W. Jones, *ChemCatChem*, 2023, **15**, e202201396.
43. Y. Guo, M. Wang, Q. Zhu, D. Xiao and D. Ma, *Nature Catalysis*, 2022, **5**, 766-776.
44. J. E. McMurry, *Organic Chemistry, 9th ed*, Cengage Learning: Boston, MA, , 2015.
45. G. Krylova, N. M. Dimitrijevic, D. V. Talapin, J. R. Guest, H. Borchert, A. Lobo, T. Rajh and E. V. Shevchenko, *Journal of the American Chemical Society*, 2010, **132**, 9102-9110.
46. M. D. Mizrahi, G. Krylova, L. J. Giovanetti, J. M. Ramallo-López, Y. Liu, E. V. Shevchenko and F. G. Requejo, *Nanoscale*, 2018, **10**, 6382-6392.
47. D. L. C. Nelson, M. M., *Lehninger Principles of Biochemistry*, Macmillan Learning, 8th ed edn., 2021.
48. H. Tian, Z. Lu, D. Li and J. Hu, *Food Chemistry*, 2018, **248**, 78-85.
49. P. Claus, *Topics in Catalysis*, 1998, **5**, 51-62.
50. C. Vericat, M. E. Vela, G. Corthey, E. Pensa, E. Cortés, M. H. Fonticelli, F. Ibañez, G. E. Benitez, P. Carro and R. C. Salvarezza, *RSC Advances*, 2014, **4**, 27730-27754.
51. E. G. Palacios, G. Juárez-López and A. J. Monhemius, *Hydrometallurgy*, 2004, **72**, 139-148.

52.I. M. Arafa, H. M. Goff, S. S. David, B. P. Murch and L. Que, Jr., *Inorganic Chemistry*, 1987, **26**, 2779-2784.
53. J. A. Horsley, *The Journal of Chemical Physics*, 1982, **76**, 1451-1458.
54.X. Han, X. Wu, Y. Deng, J. Liu, J. Lu, C. Zhong and W. Hu, *Advanced Energy Materials*, 2018, **8**, 1800935.
55. F. Delbecq and P. Sautet, *Journal of Catalysis*, 1995, **152**, 217-236.
56. C. Amiens, D. de Caro, B. Chaudret, J. S. Bradley, R. Mazel and C. Roucau, *Journal of the American Chemical Society*, 1993, **115**, 11638-11639.
57. C. N. Kostelansky, J. J. Pietron, M.-S. Chen, W. J. Dressick, K. E. Swider-Lyons, D. E. Ramaker, R. M. Stroud, C. A. Klug, B. S. Zelakiewicz and T. L. Schull, *The Journal of Physical Chemistry B*, 2006, **110**, 21487-21496.
58. P. Hu, L. Chen, X. Kang and S. Chen, *Accounts of Chemical Research*, 2016, **49**, 2251-2260.
59. A. Kumar, K. Dhar, S. S. Kanwar and P. K. Arora, *Biological Procedures Online*, 2016, **18**, 2.
60.J. Park, An, K., Hwang, Y., Park, J.-G., Noh, H.-J., Kim, H.-J., Park, J.-H., Hwang, N.-M., Hyeon T., *Nature Materials*, 2004, **3**, 891 - 895.
61. B. Ravel and M. Newville, *Journal of Synchrotron Radiation*, 2005, **12**, 537-541.
62. G. Kresse and J. Furthmüller, *Physical Review B*, 1996, **54**, 11169-11186.
63. J. P. Perdew, K. Burke and M. Ernzerhof, *Physical Review Letters*, 1996, **77**, 3865-3868.
64. P. E. Blöchl, *Physical Review B*, 1994, **50**, 17953-17979.
65. G. Kresse and D. Joubert, *Physical Review B*, 1999, **59**, 1758-1775.
66.G. Henkelman, A. Arnaldsson and H. Jónsson, *Computational Materials Science*, 2006, **36**, 354-360.

Data availability

The data supporting this article have been included as part of the ESI.